THE JOURNAL OF PHYSICAL CHEMISTRY C

Article

Cite This: J. Phys. Chem. C 2017, 121, 25509-25519

pubs.acs.org/JPCC

Emergence of Nonlinear Optical Activity by Incorporation of a Linker Carrying the *p*-Nitroaniline Motif in MIL-53 Frameworks

Karen Markey,[†,▽] Martin Krüger,[‡,▽] Tomasz Seidler,[§,∥,▽] Helge Reinsch,[‡] Thierry Verbiest,[⊥] Dirk E. De Vos,[†] Benoît Champagne,[*,∥] Norbert Stock,[*,‡] and Monique A. van der Veen[*,#]

[†]Centre for Surface Chemistry and Catalysis, Faculty of Bioscience Engineering, University of Leuven, 3001 Leuven, Belgium

[‡]Institut für Anorganische Chemie, Christian-Albrechts-Universität zu Kiel, 24118 Kiel, Germany

[§]K. Gumiński Department of Theoretical Chemistry, Jagiellonian University, Romana Ingardena 3, 30-060 Kraków, Poland

[∥]Unité de Chimie Physique Théorique et Structurale, University of Namur, 5000 Namur, Belgium

[⊥]Molecular Imaging and Photonics, KU Leuven − University of Leuven, 3001 Leuven, Belgium

[#]Catalysis Engineering, Department of Chemical Engineering, Delft University of Technology, 2629 Delft, The Netherlands

Supporting Information

ABSTRACT: *p*-Nitroaniline presents the typical motif of a second-order nonlinear optically (NLO) active molecule. However, because of its crystallization in an antiparallel and hence centrosymmetric structure, the NLO activity is lost. In this contribution, the *p*-nitroaniline motif was built successfully into the MIL-53 metal−organic framework. More precisely, MIL-53 was synthesized with 2-amino-5-nitroterephthalate as organic linker, with Al^{3+}, Ga^{3+}, or In^{3+} as inorganic cation. The Al and Ga structures are polar, as confirmed by second-harmonic generation microscopy, yielding stable NLO materials. Indeed, they contain a 22−36% surplus of the dipolar 2-amino-5-nitro-terephthalate oriented in a parallel fashion. The indium compound was shown to be less crystalline and centrosymmetric. Ab initio modeling of the second-order NLO response shows that the Al and Ga materials show a response comparable to typical inorganic commercial NLO materials such as KDP. As a hybrid material, capable of low-temperature synthesis and processing and the ultrafast NLO responses associated with organic materials, this material can potentially provide an interesting venue for applications with respect to traditional inorganic NLO materials.

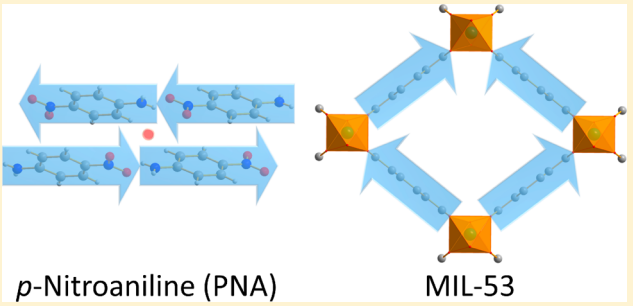

INTRODUCTION

Polar crystalline materials can be used for a wide range of applications because they possess characteristics such as piezoelectricity, pyroelectricity, second-order nonlinear optical (SONLO) activity, and, in the case of reversible polarity, ferroelectricity.[1−3] SONLO activity specifically can be applied for telecommunication, information storage, optical switching, and signal processing.[4] Currently, mainly polar inorganic materials are used in commercial applications. However, inorganics have several limitations, with the limitations depending on the envisioned application.[5] A general limitation of inorganic crystals is that their properties can hardly be fine-tuned through chemical synthesis. Organic materials, on the contrary, are tunable and can be processed in more versatile ways.[5,6] However, organic polar molecules have the disadvantage of typically crystallizing in an antiparallel orientation due to the optimization of dipole−dipole interactions, which cancels the overall dipole moment.[5,7,8] To achieve polar alignment of the organic entities, methods such as poling of polymers, Langmuir−Blodgett films, or self-assembled monolayers are required.[9−14] Crystal engineering methods can also be used to bypass the problem of centrosymmetric organization in organic materials. This is achieved by, for example, crystallization of chiral compounds[15] or by cocrystallization with chiral components resulting in noncentrosymmetric polymorphs.[16−18]

Metal−organic frameworks (MOFs) or porous coordination polymers (PCPs) are a promising category of materials that are highly tunable and that can circumvent the tendency of organic molecules to organize in a nonpolar fashion.[5] MOFs are porous hybrid materials composed of metal ions or metal clusters and organic linkers. MOFs are tunable because the metal nodes can be varied, the organic linkers can be chemically engineered, and the adsorbates in the pores can be exchanged. Polar organization in MOFs can be attained via several strategies. A first strategy to obtain noncentrosymmetric and potentially polar MOFs is to choose a metal−organic coordination bond geometry that does not allow centrosymmetric organization. Typical examples of this strategy are diamonoid frameworks[7,19] and MOFs with nicotinate as a linker.[20] As a second strategy,

Received: September 18, 2017
Revised: October 11, 2017
Published: October 17, 2017

DOI: 10.1021/acs.jpcc.7b09190
J. Phys. Chem. C 2017, 121, 25509−25519

polar linkers can potentially organize in a polar fashion due to optimal interactions and steric hindrance keeping the linkers in place. An example of this strategy is the insertion of 2-aminoterephtalate in MIL-53.[21] A third strategy to obtain polarity in MOFs is via polar ordering of guest species in the frameworks' pores, as seen in perovskite structure type MOFs, where nitrogen-containing cations are ordered in a polar way in the cavities.[22−25] Also, neutral polar species, such as water, can organize in a polar fashion in MOFs.[26,27] A fourth strategy to create polar MOFs is the incorporation of an electronegative ion in the framework structure. An example exploiting this strategy is the fluoride doping of MIL-53(Fe), which, together with the guest molecules, results in polar organization.[28]

In this research, we want to incorporate the well-studied polar *p*-nitroaniline (PNA) motif in a MOF to potentially organize the linker in a polar organization that can be maintained. The organic PNA molecule is the poster-child polar push−pull molecule for second-order nonlinear optics, generating frequency doubled light. However, crystallization of the molecule leads to the aforementioned antiparallel organization, removing the polarity.[29,30] To obtain a polar material benefiting from the SONLO properties of PNA, researchers successfully adsorbed PNA molecules into zeolites, leading to overall polarity.[31−36] However, zeolites have limited chemical modification and processing possibilities. MOFs can alleviate these issues, as they offer tunability, combined with ease of processing and the possibility to obtain polarity. In addition, when a flexible framework such as MIL-53 is chosen, opportunities arise to fine-tune the polarization by variation of the pore openings. In this contribution, for the first time, a polar organization of the well known PNA motif was created via the strategy of creating a linker carrying the PNA motif and incorporating it in several MIL-53 frameworks, yielding highly stable polar and second-order nonlinear optically active materials.

EXPERIMENTAL SECTION

Synthesis. The chemicals used for the synthesis were commercially available and were used without further purification. Gallium and indium salts were purchased at ABCR and used as received. The 2-amino-5-nitroterephthalic acid (**H_2BDC-NH_2/NO_2**) linker was synthesized by a three-step synthesis procedure based on literature published by Skibo et al.[37] Following the literature procedure, starting with the hydrolysis of dimethyl aminoterephthalate to 2-aminotereph-thalic acid, the product was reacted with formamide (HC(O)-NH_2) to give 2-formamido terephthalic acid. After nitration of this intermediate, the final H_2BDC-NH_2/NO_2 linker was obtained by deprotection. Following the synthesis procedure, single crystals of 2-amino-5-nitroterephthalic acid could be obtained after recrystallization from hot water. The purity of the H_2BDC-NH_2/NO_2 linker was confirmed by ^{1}H NMR spectroscopy. More details of the synthesis and characterization can be found in the Supporting Information (SI) (Figures S1−S5). A flowchart displaying synthesis pathways, sample treatments and corresponding sample names is shown in Figure 1.

Using three different metals (aluminum, gallium, indium), discovery and synthesis optimization of MIL-53 frameworks was carried out employing our 24-high-throughput (HT) reactor system for solvothermal reactions, allowing a fast and efficient determination of optimal reaction parameters.[38−41] The reactor system contains custom-made Teflon reaction

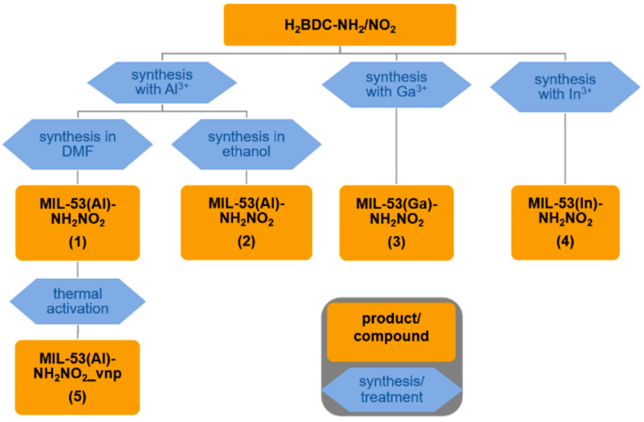

Figure 1. Flowchart of experiments showing synthesis pathways, sample treatments, and corresponding sample names.

vessels with a maximum volume of 2 mL. For our M^{3+}/H_2BDC-NH_2/NO_2/solvent/additive (M = Al, Ga, In) system the following parameters were investigated: the molar ratio M^{3+}:H_2BDC-NH_2/NO_2, reaction solvents, volumetric ratio of solvent/water mixture, reaction temperature, reaction time, reaction vessel size, and the addition of 2 M HNO_3 or 2 M NaOH solution. Detailed information on the reactions carried out can be found in Tables S1−S4. MIL-53(Al)-NH_2/NO_2 was synthesized by two different routes: one using DMF/H_2O as solvent and one with ethanol/H_2O as solvent. MIL-53(Al)-NH_2/NO_2 in DMF, denoted as **MIL-53(Al)-NH_2/NO_2 (1)**, was synthesized with the following optimized synthesis conditions: To a mixture of 44.2 μL of 2 M $AlCl_3$·$6H_2O$ (88.4 μmol) in H_2O and 20 mg 2-amino-5-nitroterephthalic acid (H_2BDC-NH_2/NO_2, 88.4 μmol), 60 μL of DMF (0.78 mmol), 32.5 μL of H_2O (1.8 mmol), and 13.3 μL of 1 M NaOH (13.3 μmol) in H_2O were added to a 2 mL Teflon reactor. The reactor was sealed carefully and heated to 150 °C within 1 h, held at this temperature for 36 h, and then cooled to room temperature within 1 h. The product was filtered off, stirred in 10 mL of *N*,*N*-dimethylformamide (DMF) at room temperature for 2 h, filtered off again, and dried under ambient conditions. As an alternative route, MIL-53(Al)-NH_2/NO_2 was prepared in ethanol, denoted as **MIL-53(Al)-NH_2/NO_2 (2)**, with the following optimized synthesis conditions: 21.4 mg of $AlCl_3$·$6H_2O$ (88.4 μmol), 20 mg of H_2BDC-NH_2/NO_2, (88.4 μmol), 125 μL (2.1 mmol) of ethanol, and 25 μL (1.4 mmol) of H_2O were added in a 2 mL Teflon reactor. The reactor was heated to 150 °C within 1 h, held at this temperature for 36 h, and cooled to room temperature within 1 h. Obtained products were filtered off and dried under ambient conditions. Compound **MIL-53(Ga)-NH_2/NO_2 (3)** was synthesized with the following optimized synthesis conditions: To a mixture of 21.4 μL of 2 M $Ga(NO_3)_3$·H_2O (43 μmol) in H_2O and 20 mg H_2BDC-NH_2/NO_2 (88.4 μmol), 60 μL of DMF (0.78 mmol), 25.8 μL of ethanol (0.44 mmol), and 20 μL of 1 M HNO_3 (20 μmol) in H_2O were added in a 2 mL Teflon reactor. The reactor was sealed carefully and heated to 150 °C within 1 h, held at this temperature for 16 h, and then cooled to room temperature within 1 h. The product was filtered off and dried under ambient conditions. Compound **MIL-53(In)-NH_2/NO_2 (4)** was synthesized with the following optimized synthesis conditions: To a mixture of 44.2 μL of 2 M $In(NO_3)_3$·H_2O (88.4 μmol) in DMF and 10 mg H_2BDC-NH_2/NO_2 (44.2 μmol), 85.8 μL of DMF (1.12 mmol) and 20 μL of ethanol

DOI: 10.1021/acs.jpcc.7b09190
J. Phys. Chem. C 2017, 121, 25509−25519

(0.34 mmol) were added in a 2 mL Teflon reactor. The reactor was sealed carefully and heated to 150 °C within 1 h, held at this temperature for 16 h, and then cooled to room temperature within 1 h. The product was filtered off and dried under ambient conditions.

Thermal Activation. Prior to the sorption experiments the samples **1**−**4** were activated at 200 °C for 16 h under reduced pressure (10^{-2} kPa). For MIL-53(Al)-NH_2/NO_2 (**1**) this activation procedure was carried out twice, ultimately resulting in **MIL-53(Al)-NH_2/NO_2_vnp (5)**, the very narrow pore form of MIL-53(Al)-NH_2/NO_2 (**1**).

Structural Characterization. The high-throughput PXRD measurements were performed in transmission geometry using a STOE HT diffractometer equipped with a *xy* stage and an image plate detector system (Cu $K_{\alpha 1}$ radiation). Collection of high-resolution powder diffraction data was performed with a STOE Stadi-P powder diffractometer equipped with a MYTHEN1K detector system (Cu $K_{\alpha 1}$ radiation). Single-crystal X-ray diffraction data were collected on a Bruker P4 diffractometer equipped with a IPSD detector using Mo K_α radiation. The structural models for the Rietveld refinement for MIL-53(Al)-NH_2/NO_2 (**1**) and MIL-53(Ga)-NH_2/NO_2 (**3**) were obtained as follows: The cell parameters were obtained by indexing laboratory high-resolution X-ray powder diffraction data using TOPAS Academic v4.1,[42] indicating strong similarity of the title compound with the hydrated form of Al-MIL-53-np.[43] Using the Accelrys Materials Studio 4.1 software package, the BDC^{2-} molecule in MIL-53 was exchanged by BDC-NH_2/$NO_2{}^{2-}$.[44] The lattice parameters were fixed to the experimentally determined values, and energy minimization calculations were carried out using the universal force-field (UFF) as implemented in the Forcite module of Materials Studio.[44]

General Characterization. Scanning electron microscopy (SEM) images were recorded on a JSM-6010PLUS/LA instrument from JEOL after sputter coating with palladium−gold. ^{1}H NMR spectroscopy was carried out on a Bruker DRX 500 at 200 MHz. Thermogravimetric analyses were performed using a NETZSCH STA 409 CD analyzer. The samples were heated in Al_2O_3 crucibles at a rate of 4 K min^{-1} under a flow of synthetic air (75 mL·min^{-1}). The TG data were corrected for buoyancy and current effects. A HEKAtech Euro Elemental Analyzer was used for elemental analysis. Sorption experiments were carried out using a Belsorp-max instrument (BEL JAPAN). The characterization of the compounds was carried out using as-synthesized (for **2** to **4**) or washed samples (for **1**).

SONLO Measurements. The compounds were always measured in their as-synthesized form, unless mentioned otherwise. Second harmonic generation (SHG) scanning microscopy images were recorded on a multiphoton laser scanning microscope (FV1200MPE, BX61WI frame, Olympus) in transmission mode. The microscope was equipped with a 50× long working distance objective (SLMPlan N, NA = 0.35, Olympus) and a visible-light condenser (NA = 0.9, Olympus). To select the 400 nm SHG light a dichroic mirror and band-pass filter combination was used (T425lpxr-et405/10bp of Chroma). As the laser source, a femtosecond tunable laser operating at a wavelength of 800 nm was used (∼100 fs pulse duration, 80 MHz pulse rate) (Insight DeepSee, Spectra-Physics). The laser light was linearly polarized using a Glan-Taylor polarizer, and the plane of polarization was controlled via a zero-order half-wave plate from Thorlabs. The quantification of the second-order NLO activity was done using a customized inverted wide-field SHG microscope (IX71 frame, Olympus), which operates in transmission mode. To be able to consider the incident light as a collimated beam, a long focal length lens (f = 75 mm, NA = 0.013) was used. Images were formed by a 15× long working distance objective (LMU-15×-NUV, NA = 0.32, Thorlabs) and recorded with an EM-CCD camera (Hamamatsu). To select the 400 nm SHG light a filter set consisting of a bandpass filter (BG39, 2 mm, Schott) and an interference filter (F10-100, center wavelength 400 nm, fwhm 10 nm, Melles Griot) was used. As the laser source, a Ti:sapphire laser operating at a wavelength of 800 nm was used (∼100 fs pulse duration, 80 MHz pulse rate) (Tsunami, Spectra-Physics) combined with a pump laser (Millenia Pro, Spectra-Physics). The laser light was linearly polarized using a Glan-Taylor polarizer, and the plane of polarization was controlled via a zero-order half-wave plate from Thorlabs. All SHG images were processed with ImageJ and Fiji software.

Multiscale Ab Initio/Local Field Theory Calculations to Determine $\langle d_{\text{eff}} \rangle$. For both MIL-53(Al)-$NH_2$/$NO_2$ and MIL-53(Ga)-NH_2/NO_2 compounds two crystal phases (A and C, see Figure 4) were considered in the calculations for $\langle d_{\text{eff}} \rangle$. These phases (as well as vnp MIL-53(Al)-NH_2) were first considered as independent pure phases for geometry optimization using periodic boundary conditions (PBC) within the CRYSTAL14 package.[45,46] The optimizations were performed at the density functional theory (DFT) level of theory with the B3LYP exchange-correlation functional and the 6-31G(d,p) basis set. Only the fractional coordinates were optimized with the cell parameters kept fixed at their experimental values. Using these optimized geometries, the calculations of the molecular properties, the polarizability, α, and the first hyperpolarizability, β, were performed for the individual cations and anions within their embedding crystal field. These fields were simulated with a 100 Å radius sphere of Mulliken point charges obtained from PBC/B3LYP calculations at the optimized crystal geometries.[47] The static ($\lambda = \infty$) responses were computed at the second-order Møller−Plesset (MP2) level of theory with 6-311++G(d,p) basis set. The dynamic MP2 responses were then calculated following a multiplicative approximation that combines static and dynamic B3LYP/6-311++G(d,p) responses to describe frequency dispersion.[48] All of the molecular property calculations were performed with Gaussian09 software.[49] Using the molecular properties, the linear susceptibilities, $\chi^{(1)}$, and therefore the refractive indices, n, and the second-order nonlinear susceptibilities, $\chi^{(2)}$, were then calculated by employing the local field theory (LFT) methodology,[50−55] recently applied to MOFs.[48] Finally, the effective values, $\langle d_{\text{eff}} \rangle$, were evaluated after accounting for the weights of the different crystal forms for phase-matching conditions as well as for the averaging over all light polarization orientations with respect to the crystal grains. The d_{eff} values are related to the $\chi^{(2)}$ tensors by the following equation

$$d_{\text{eff}} = \frac{1}{2}\underline{e}_i(2\omega)\cdot\underline{\underline{\chi}}^{(2)}:\ \underline{e}_j(\omega)\,\underline{e}_k(\omega) \times \text{sinc}\left(\frac{\Delta k\, r}{2}\right) \quad (1)$$

where $\underline{e}_i$, $\underline{e}_j$, and $\underline{e}_k$ are the light-wave polarization vectors, r is the optical path length (symbolizing the grain size in the calculation), and

$$\Delta k = \frac{2\pi}{\lambda}\Delta n;\ \ \Delta n = 2n_{2\omega}^{1} - n_{\omega}^{2} - n_{\omega}^{3} \quad (2)$$

DOI: 10.1021/acs.jpcc.7b09190
J. Phys. Chem. C 2017, 121, 25509−25519

is the phase mismatch related to the difference of refractive indices. The indices 1, 2, and 3 in Equation 2 refer the crystal axes. Equation 1 accounts for (i) the biaxial nature of the crystal and the fact that nonpolarized light beams split into two perpendicularly polarized [called (+) and (−)] beams propagating at different speeds and for (ii) the interaction between the incident light at fundamental frequency [(+) or (−)] and the generated light [also (+) or (−)] at twice its frequency. Finally, all possible orientations of the light-wave polarizations with respect to the crystal grains, defined by the polar angles (θ, ϕ), are taken into account to estimate the average $\langle d_{eff} \rangle$ quantities. More details of the whole multiscale method, including the evaluation of the local field, the treatment of the frequency dependence of the linear and nonlinear responses,[48,56] and the selection of the charges to describe the in-crystal polarization field[47] are provided in the SI.

RESULTS AND DISCUSSION

For our purpose to create functional polar crystals by incorporation of the PNA motif into a MOF, we started by designing a suitable linker molecule. As the aimed framework structure, we chose MIL-53 because the flexibility of the framework can potentially allow fine-tuning of the polarization by variation of the pore opening. For the linker molecule to benefit from similar polar and SONLO properties as PNA, the linker was designed containing an extended π-conjugated system with amino and nitro donor and acceptor groups. To ensure that the linker can form metal coordination bonds to create a MIL-53 framework, opposing carboxylate ends were added to the aromatic ring. This resulted in the 2-amino-5-nitroterephthalic acid (H_2BDC-NH_2/NO_2) molecule (Figure 2).

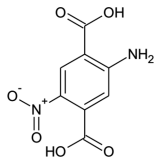

Figure 2. 2-amino-5-nitroterephthalic acid (H_2BDC-NH_2/NO_2) linker molecule.

After successful synthesis of the 2-amino-5-nitroterephthalic acid linker (Figures S1−S5), three different metals were used as the nodes to build up the aimed MIL-53 frameworks: aluminum, gallium, and indium. All frameworks were synthesized with DMF/H_2O as the solvent, and for the aluminum MOF also a synthesis in ethanol/H_2O was tested. The resulting synthesized compounds are denoted as follows: MIL-53(Al)-NH_2/NO_2 (**1**) for the aluminum compound synthesized in DMF, MIL-53(Al)-NH_2/NO_2 (**2**) for the aluminum compound synthesized in ethanol, MIL-53(Ga)-NH_2/NO_2 (**3**) for the gallium compound synthesized in DMF, and MIL-53(In)-NH_2/NO_2 (**4**) for the indium compound synthesized in DMF. The syntheses of the aluminum compounds **1** and **2** both resulted in microcrystalline powders, with the crystals from the DMF synthesis (**1**) having a more or less rectangular shape with lengths around 10 μm and thicknesses around 2 μm or a cubic shape between 0.5 and 2 μm in size (Figure 3a). The synthesis of the aluminum compound in ethanol (**2**) resulted in longer (between 10 and 50 μm) and thicker (~8 μm) crystals than the DMF synthesis (Figure 3b). The gallium compound **3** was also obtained as a

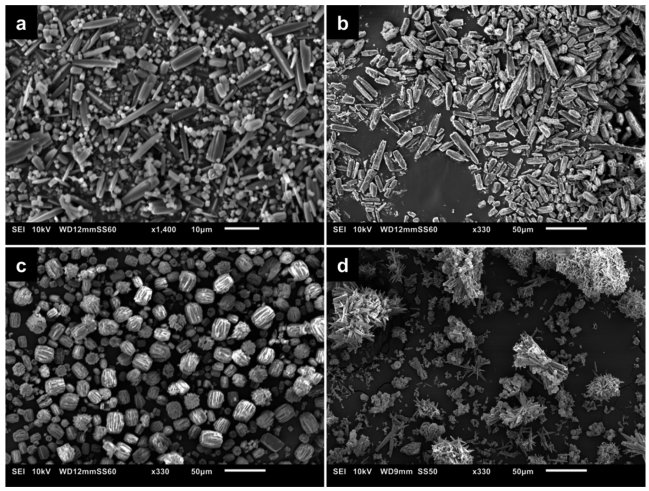

Figure 3. SEM images of H_2BDC-NH_2/NO_2 containing MOFs: (a) MIL-53(Al)-NH_2/NO_2 (**1**), (b) MIL-53(Al)-NH_2/NO_2 (**2**), (c) MIL-53(Ga)-NH_2/NO_2 (**3**), and (d) MIL-53(In)-NH_2/NO_2 (**4**). Note that the first image has a scale bar of 10 μm, whereas the other images have a scale bar of 50 μm.

microcrystalline powder, seemingly composed of aggregates of rectangular crystals grown alongside each other, with the larger aggregates having a length between 20 and 30 μm and a thickness around 20 μm (Figure 3c). The indium compound **4** appeared to be less crystalline, as the PXRD pattern did exhibit fewer well-resolved reflections (Figure 3d and Figure S10 PXRD). Additional SEM images can be found in the SI (Figures S17−S20).

Crystal Structures. To determine whether the crystal structures of compounds **1**−**4** are polar, PXRD measurements were performed to refine the structures using the Rietveld method because the compounds could only be obtained as microcrystalline powders. MIL-53(Al)-NH_2/NO_2 (**1**) and MIL-53(Ga)-NH_2/NO_2 (**3**) were confirmed to crystallize in the polar monoclinic space group *Cc* (Figures S6 and S8, containing Rietveld and Pawley refinements). The pattern of MIL-53(Al)-NH_2/NO_2 (**2**) exhibited fewer well-resolved reflections (Figure S7) and therefore a reliable refinement by Rietveld methods was not possible. However, corresponding to the Pawley refinements, the cell parameters of MIL-53(Al)-NH_2/NO_2 (**2**) hardly differ from those of MIL-53(Al)-NH_2/NO_2 (**1**) (Table 1). Because of the lower crystallinity of MIL-53(In)-NH_2/NO_2 (**4**), only the cell parameters could be obtained via indexing the powder pattern and refining them using the Pawley method (Figure S10). Because no structural refinement was possible, the indium compound could not be unambiguously assigned to a centrosymmetric or noncentrosymmetric space group. The crystallographic data of the different MIL-53-NH_2/NO_2 compounds are summarized in Table 1.

According to the results of the Rietveld refinement, structures **1**, **2**, and **3** are disordered and hence have multiple linker alignments. Therefore, ab initio calculations were performed to optimize potential framework models. As all carbon atoms of the aromatic ring are crystallographically independent in the observed noncentrosymmetric space group, depending on the substitution pattern of the linker, four different possible orientations result for the periodic crystal structure. This leads to four models, as shown in Figure 4, each containing one orientation of amino and nitro groups. Note

DOI: 10.1021/acs.jpcc.7b09190
J. Phys. Chem. C 2017, 121, 25509−25519

Table 1. Crystallographic Data of the Title Compounds

	MIL-53(Al)-NH_2/NO_2 (**1**)	MIL-53(Al)-NH_2/NO_2 (**2**)	MIL-53(Ga)-NH_2/NO_2 (**3**)	MIL-53(In)-NH_2/NO_2 (**4**)
formula sum	$[Al(OH)(BDC\text{-}NH_2/NO_2)]$	$[Al(OH)(BDC\text{-}NH_2/NO_2)]$	$[Ga(OH)(BDC\text{-}NH_2/NO_2)]$	$[In(OH)(BDC\text{-}NH_2/NO_2)]$
method	Rietveld	Pawley	Rietveld	Pawley
wavelength	Cu $K_{\alpha1}$	Cu $K_{\alpha1}$	Cu $K_{\alpha1}$	Cu $K_{\alpha1}$
a/Å	17.5669(8)	17.565(5)	17.460(1)	16.870(8)
b/Å	13.3691(7)	13.469(3)	14.1006(7)	13.948(7)
c/Å	6.6105(2)	6.616(2)	6.7350(2)	7.235(4)
β/deg	112.125(3)	112.273(8)	112.712(6)	90
spacegroup	*Cc*	*Cc*	*Cc*	*Imam* or *Ima2*
R_{wp} (%)	5.57	3.79	7.41	4.20
R_{Bragg} (%)	1.56		2.81	
GoF	2.11	1.74	2.00	1.54

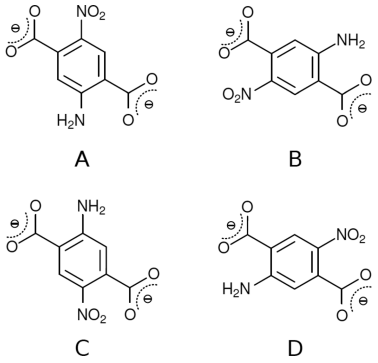

Figure 4. Different positions of the amino and nitro groups in the BCD^{2-} anion postulated in the MIL-53-(Al)-NH_2/NO_2 structure.

that Figure 4 represents only a 2D projection of the linker; in the 3D framework the linker molecules are fixed regarding orientation, and thus four different polymorphs can be observed.

Consecutively, PXRD patterns were simulated from these models and compared against the Rietveld refinements of the experimental PXRD data. The comparison revealed that two of these models were reasonably well matching the experimental PXRD data, namely, phases A and C. As a last step, the occurrence of combinations of phase A and C was considered. The phase percentages were obtained by refining the occupancy factors and led to the conclusion that the A phase is present in excess over the C phase, which represents its oppositely oriented counterpart, respectively. Optimization of the MIL-53(Al)-NH_2/NO_2 (**1**) structure resulted in the prediction of a 61:39 ratio of phases A and C (respectively) of linker organization (Figure 5). For MIL-53(Al)-NH_2/NO_2 (**2**) the modeling procedure could not be performed, as a reliable Rietveld refinement was not possible for the experimental PXRD pattern. For MIL-53(Ga)-NH_2/NO_2 (**3**) a 68:32 ratio of phases A and C (respectively) of linker organization resulted in the best fit with the experimental PXRD patterns (Figures S8 and S9).

Additional Characterization. To further characterize the new MIL-53-NH_2/NO_2 compounds, the composition and thermal stability of **1**−**4** were verified by elemental analysis and TG measurements. All samples are stable up to ca. 300 °C, and up to this temperature occluded solvent molecules are removed from the framework (Figures S13−S15). The thermal stability is in the same range as known for other as-synthesized functionalized MIL-53 derivatives (−Cl, −Br, CH_3, NO_2, $-NH_2$, −OH).[57] The sum formulas of the compounds deduced

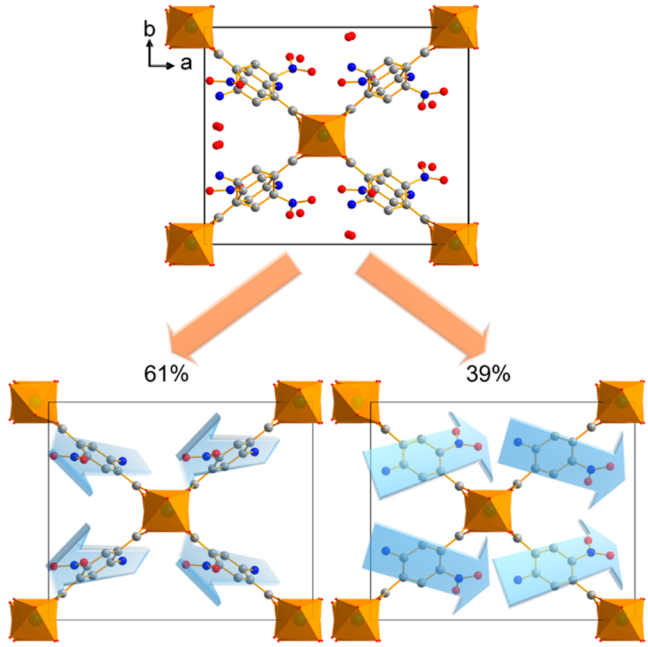

Figure 5. Crystal structure of MIL-53(Al)-NH_2/NO_2 (**1**) along [001]. The disorder (above) of the linker molecules in the structure contains 61% of the NO_2 groups of the linker molecules showing out of the plane and 39% pointing in plane. Carbon atoms are shown in gray, oxygen in red, nitrogen in blue and AlO_6 polyhedra in orange.

from the TG measurements are in good agreement with the values obtained by elemental analyses (Table S6). Solution ^1H NMR spectra show that 15% of the amino groups of **2** were ethylated during synthesis (Figures S21−S23). Because there is a large interest for the use of MOFs in sorption applications, the sorption properties of the new MIL-53 compounds **1**−**4** were also assessed. Prior to the sorption experiments all samples were activated by means of a temperature treatment to remove the guest molecules. Nitrogen sorption measurements reveal a Type I isotherm for MIL-53(Al)-NH_2/NO_2 (**1**), with a specific surface area (BET) of $a_{s,BET}$ = 287 m^2g^{-1} and a micropore volume of $V_{mic,BET}$ = 0.11 cm^3g^{-1} (Figure S24). When MIL-53(Al)-NH_2/NO_2 (**1**) was subjected to two consecutive activation treatments instead of one treatment, a very narrow pore form of MIL-53(Al)-NH_2/NO_2 (**1**) was achieved (Figure 1), as shown by the PXRD pattern (Figure S11; Table S5) and denoted as **MIL-53(Al)-NH_2/NO_2_vnp** (**5**).[58] One activation cycle probably leads to an incomplete removal of the occluded solvent molecules and the channels of

DOI: 10.1021/acs.jpcc.7b09190
J. Phys. Chem. C 2017, 121, 25509−25519

the flexible framework remain accessible. Two activation cycles fully remove all guest molecules, which leads to a framework contraction, most likely induced by attractive forces between adjacent linker molecules. These intraframework interactions are apparently exceeded by host−guest interactions in the solvent-filled MOF. Nitrogen sorption measurements for this very narrow pore form **5** show that the values reduce to $a_{s,BET}$ = 92 $m^2 g^{-1}$ and $V_{mic,BET}$ = 0.04 $cm^3 g^{-1}$. Immersion of the very narrow pore compound **5** in DMF results in a re-establishment of the structure to the as-synthesized MIL-53(Al)-NH_2/NO_2 (**1**) structure with the wider pores (Figure S12). Additionally, water, CO_2, and hydrogen sorption experiments were performed on compound **1** (Figures S25−S27), starting from the sample that received one activation treatment. The measurements reveal a very hydrophilic character of compound **1**, with a total uptake of 12 wt % H_2O (at 1 bar and 298 K), whereas 9 wt % of CO_2 (1 bar, 298 K) and 0.7 wt % of hydrogen (1 bar, 77 K) can be adsorbed. The uptake of CO_2 of ca. 90 mg/g in MIL-53(Al)-NH_2/NO_2 (**1**) is comparable to the reported uptake of MIL-53(Al) of ∼106 mg/g and MIL-53(Al)-NH_2 of ∼98.6 mg/g.[59,60] Compounds **2**−**4** did not show any uptake of N_2; therefore, no other types of sorption measurements were carried out for these compounds.

Second Harmonic Generation Activity. The PXRD refinements revealed that polar symmetries are achieved due to a net polar organization of the linkers in compounds MIL-53(Al)-NH_2/NO_2 (**1**), MIL-53(Al)-NH_2/NO_2 (**2**), and MIL-53(Ga)-NH_2/NO_2 (**3**). Because polar materials can display interesting second harmonic generation (SHG) activity, the occurrence of SHG was probed locally through SHG microscopy on single crystals of the compounds.

SHG is a nonlinear optical process, taking place when high-intensity laser light interacts with materials possessing a noncentrosymmetric organization.[61] This noncentrosymmetric requirement for SHG to occur is a consequence of the nature of the process. The SHG process converts the energy and momentum of two photons into one photon with doubled frequency, by a coherent process, meaning phase relations between the photons are important. By consequence, destructive interference of SHG occurs in centrosymmetric organized materials, as the related third-rank tensor for the second-order nonlinear susceptibility $\chi^{(2)}$ becomes zero. For noncentrosymmetric organizations, constructive interference of the SHG process occurs, and an SHG signal can be detected. Therefore, SHG microscopy can be used as a tool to distinguish noncentrosymmetric from centrosymmetric organizations. In our case, this allows us to locally probe areas in the crystals where noncentrosymmetric linker alignments are occurring.

Complementary to the SHG images, two-photon fluorescence (2PF) images were recorded. Two-photon fluorescence also is a nonlinear optical process, taking place when fluorophores are irradiated with high-intensity laser light.[61] In 2PF, two photons nearly simultaneously excite a fluorophore, which, in turn, emits a fluorescence photon. The process is an incoherent process because the excitation and emission events are separated in time and phase relations between the emitted versus exciting photons are absent. Because there is no symmetry requirement for the process to occur, fluorophores can be visualized regardless of their organization.[62] In our case, the linker with PNA motif acts as the fluorophore. By comparing SHG and 2PF images, areas with noncentrosymmetric linker organizations (visible in both SHG and 2PF images) can be distinguished from areas with random linker organizations (only visible in 2PF images).

From Figure 6 it is clear that compounds MIL-53(Al)-NH_2/NO_2 (**1**), MIL-53(Al)-NH_2/NO_2 (**2**), and MIL-53(Ga)-NH_2/NO_2 (**3**) contain areas displaying SHG activity. Those areas thus contain noncentrosymmetric linker organizations, more specifically polar alignments, as determined by the PXRD refinements. Comparison of SHG and 2PF images clearly shows that the two-photon fluorescence signal is more homogeneously distributed than the SHG signal. This means that an overall polar linker organization is not present throughout the entire crystals. In contrast with compounds **1**−**3**, MIL-53(In)-NH_2/NO_2 (**4**) does not display SHG activity (Figure S30). Apart from the non-SHG active powder, a single particle shows SHG activity in the image. This is likely due to an impurity or minority phase. The apolar symmetry of the indium compound can be explained by the larger M−O distances in the MOF in comparison with the Al and Ga compounds (Al−O: 1.8 to 1.9 Å;[43] Ga−O: 1.8 to 2.0 Å;[63] In−O: 2.1 to 2.2 Å[64]), which allow a possible rotation, and hence randomization, of the linker molecules.

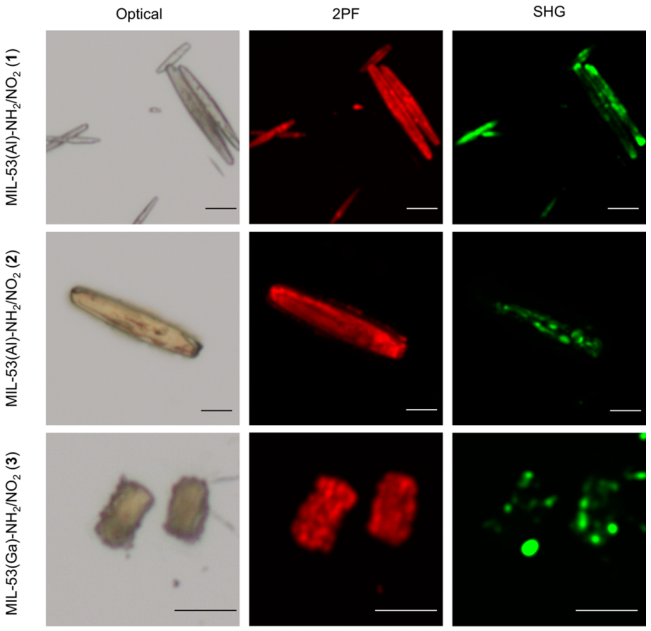

Figure 6. From left to right: optical, two-photon fluorescence, and second-harmonic generation images. From top to bottom: as synthesized MIL-53(Al)-NH_2/NO_2 (**1**), MIL-53(Al)-NH_2/NO_2 (**2**), and MIL-53(Ga)-NH_2/NO_2 (**3**). The SHG images display the average intensity of linearly polarized laser light, calculated over 60 images, each image being 3° apart in polarization direction of the incident polarized beam. The scale bars indicate a distance of 10 μm for each image.

To quantify the SHG activity of compounds **1**−**3**, the effective second-order nonlinear optical coefficient $\langle d_{eff} \rangle$ was determined experimentally for each compound. The $\langle d_{eff} \rangle$ value of a material represents the average SHG activity of a collection of crystals of the material, oriented differently in the measurements' coordinate system. Averaging over all orientations allows quantification of the SHG activity of materials for which measurements along a specific crystal axis are not straightforward, as is the case for small crystals. To obtain an absolute value for $\langle d_{eff} \rangle$, the sample crystals are measured

DOI: 10.1021/acs.jpcc.7b09190
J. Phys. Chem. C 2017, 121, 25509−25519

against a reference crystal, of which the d value is known (in our case a BBO crystal was used as the reference). Using the $\langle d_{eff} \rangle$ value for the quantification of the SHG activity of a compound, differences in crystal size and refractive index are taken into account.[65] A detailed description of the $\langle d_{eff} \rangle$ calculation is given in the SI. The experimentally determined $\langle d_{eff} \rangle$ values of compounds **1**−**3** are summarized in Table 2.

Table 2. Experimental $\langle d_{eff} \rangle$ Values

	$\langle d_{eff} \rangle$ (pm V^{-1})
MIL-53-(Al)-NH_2/NO_2 (**1**)	0.02 ± 0.01
MIL-53-(Al)-NH_2/NO_2 (**2**)	0.05 ± 0.02
MIL-53-(Ga)-NH_2/NO_2 (**3**)	0.02 ± 0.01

For the aluminum compound **1** and the gallium compound **3**, equal $\langle d_{eff} \rangle$ values were measured (0.02 pm·V^{-1}). The aluminum compound synthesized in ethanol **2** displayed a higher SHG activity, with a $\langle d_{eff} \rangle$ value of 0.05 pm·V^{-1}. An explanation for the higher SHG activity of this compound could be a higher A/C fraction (Figure 4), which would lead to more noncentrosymmetrically organized linkers. However, as mentioned previously, we could not determine the A/C fraction for compound **2** through structure refinements, as a reliable structure refinement was not possible for this compound.

Comparing the $\langle d_{eff} \rangle$ values of the MIL-53-NH_2/NO_2 MOFs **1**−**3** with the reported $\langle d_{eff} \rangle$ value of MIL-53(Al)-NH_2 (0.05 ± 0.02 pm V^{-1}),[21] for which the terephthalic acid linker is functionalized solely with an amino group, it can be concluded that the SHG activities are in the same range, despite their differences in linker functionalization. This seems counterintuitive, as a higher SHG activity for the compounds with the amino/nitro functionalized linkers could be expected because this linker possesses a more efficient donor−acceptor system, resulting in a higher hyperpolarizability, which could lead to a higher SHG activity. However, an important determining factor of the SHG efficiency is how the linkers are organized in the crystal structure. The occurrence of several phases of linker organization can lead to (partial) cancellation of the SHG activity. Additionally, MIL-53-NH_2/NO_2 and MIL-53(Al)-NH_2 reabsorb the wavelength at which SHG is generated (400 nm) most likely to a different extent (see Figure S34 and ref 66). In fact, a rough estimate of the amount of reabsorbed SHG-light is calculated in the SI for a crystal containing the PNA motif, with the same linker density as for MIL-53(Al)-NH_2/NO_2 (**1**) and a height of 2 μm. This estimation predicts a transmittance of only 2.1 × 10^{-4}% of generated 400 nm SHG light through the sample. Whereas the calculation is based on the extinction coefficient of PNA in water, rather than 2-amino-5-nitroterephthalate build into MIL-53, the majority of the generated SH-light can be expected to be reabsorbed by the MIL-53(Al)-NH_2/NO_2. To gain more insight into the differences between the MIL-53-NH_2/NO_2 compounds and the previously reported MIL-53(Al)-NH_2 compound, they need to be investigated off-resonance, which is also directly relevant for NLO applications. Hence we theoretically determined the $\langle d_{eff} \rangle$ values using ab initio calculations on the crystal structures in the next section.

Analysis of MIL-53(Al)-NH_2/NO_2 (1), MIL-53(Ga)-NH_2/NO_2 (3), and MIL-53(Al)-NH_2 SHG Activity by Ab Initio Calculations. Multiscale numerical simulations were carried out to predict and interpret the $\langle d_{eff} \rangle$ values of MIL-53(Al)-NH_2/NO_2 (**1**), MIL-53(Ga)-NH_2/NO_2 (**3**), and MIL-53(Al)-NH_2. To account for the occurrence of a combination of A and C linker phases in compounds MIL-53(Al)-NH_2/NO_2 (**1**) and MIL-53(Ga)-NH_2/NO_2 (**3**), first the $\chi^{(1)}$ and $\chi^{(2)}$ tensors for the pure phases of linker organization A and C were calculated. Consecutively, the final $\chi^{(1)}$ and $\chi^{(2)}$ tensors were obtained by accounting for the A/C phase ratios, as determined from the powder diffraction refinement, that is, 61:39 for MIL-53(Al)-NH_2/NO_2 (**1**) and 68:32 for MIL-53(Ga)-NH_2/NO_2 (**3**).

The resulting $\chi^{(1)}$ and $\chi^{(2)}$ tensors and $\langle d_{eff} \rangle$ values for MIL-53(Al)-NH_2/NO_2, MIL-53(Ga)-NH_2/NO_2, and MIL-53(Al)-NH_2 are presented in Table 3 (See also the SI for additional data on the refractive indices as well as linear and nonlinear responses for other incident wavelengths, Tables S7 and S8). It is clear that the $\chi^{(2)}_{ijk}$ tensors for the pure A and C phases are almost equal in magnitude but opposite in sign, especially for the aluminum compound MIL-53(Al)-NH_2/NO_2 (**1**). This means that the SHG-generating part (mostly the organic linker) is practically oriented antiparallel in phase A versus phase C. Moreover, if a material would contain equal amounts of phases A and C, on a scale below the diffraction limit, then practically no SHG would be generated, as the phases would cancel each other out. Because MIL-53(Al)-NH_2/NO_2 (**1**) and MIL-53(Ga)-NH_2/NO_2 (**3**) were experimentally found to contain, respectively, 61:39 and 68:32 ratios of phases A:C, the tensor components and therefore also the SHG activity are not completely canceled out, but the values are lower than those of the pure phases. Considering the largest $\chi^{(2)}$ tensor components of the pure phases, this reduction attains a factor of 4 to 5 for M = Al and 2 to 3 for M = Ga. Still, relatively high maximum $\chi^{(2)}_{ijk}$ tensor components are found for the

Table 3. MP2/LFT Results for MIL-53(Al)-NH_2/NO_2, MIL-53(Ga)-NH_2/NO_2, and MIL-53(Al)-NH_2 (in the very narrow pore phase) Calculated for an Incident Wavelength of 1064 nm (Selected $\chi^{(2)}$ Tensor Components (in pm V^{-1}) and $\langle d_{eff} \rangle$ (in pm V^{-1}))[a]

compound/phase	$\chi^{(2)}_{333}$	$\chi^{(2)}_{111}$	$\chi^{(2)}_{133}$	$\chi^{(2)}_{113}$	$\langle d_{eff} \rangle$ r = 0 μm	$\langle d_{eff} \rangle$ r = 3 μm	$\langle d_{eff} \rangle$ r = 10 μm
MIL-53(Al)-NH_2/NO_2 Phase A	133.9	−1.5	−16.3	−2.1	3.409	0.583	0.215
MIL-53(Al)-NH_2/NO_2 Phase C	−134.2	1.5	16.2	2.1	3.394	0.576	0.212
MIL-53(Al)-NH_2/NO_2 A/C (61:39)	29.3	−0.3	−3.6	−0.5	**0.751**	**0.131**	**0.048**
MIL-53(Ga)-NH_2/NO_2 Phase A	−4.4	222.2	−6.9	13.3	2.952	0.541	0.209
MIL-53(Ga)-NH_2/NO_2 Phase C	4.3	−147.1	7.0	−4.9	3.089	0.828	0.332
MIL-53(Ga)-NH_2/NO_2 A/C (68:32)	−1.3	105.0	−3.2	1.9	**1.221**	**0.272**	**0.107**
MIL-53(Al)-NH_2 (vnp)	6.2	−15.8	−6.6	−2.6	**2.130**	**0.440**	**0.178**

[a]For MIL-53(M)-NH_2/NO_2, results are listed for the pure A and C phases as well as for the A:C ratios obtained from PXRD analysis.

DOI: 10.1021/acs.jpcc.7b09190
J. Phys. Chem. C 2017, 121, 25509−25519

compounds containing mixed phases: 29.3 pm V^{-1} for $\chi^{(2)}_{333}$ (M = Al) and 105.0 pm V^{-1} for $\chi^{(2)}_{111}$ (M = Ga).

However, when calculating the $\langle d_{eff} \rangle$ values for the mixed compounds, the responses are strongly reduced, and this effect is enhanced when combined with the phase mismatch factor. These two effects can be analyzed separately by considering first the results for a hypothetical zero grain size (r = 0 in Table 3) because they include the averaging over the polar angles but not the phase-matching effects and then the results for r = 3 and 10 μm, where both effects are accounted for.

First, when only averaging d_{eff} over the polar angles to get $\langle d_{eff} \rangle$, the SHG response drops by more than 1 order of magnitude with respect to the dominant $\chi^{(2)}$ tensor components (see column r = 0 μm in Table 3). This reduction is supported by the polar maps of $d_{eff}(\theta, \phi)$ (Figure S31 of SI), which highlight the (θ, ϕ) domains that result in large $\langle d_{eff} \rangle(\theta, \phi)$ values and the fact that many (θ, ϕ) domains are associated with much smaller SHG responses. Then, while accounting for the grain size, $\langle d_{eff} \rangle$ drops quite rapidly with r (Figure 7). For r = 3 μm, the responses are already reduced by about one order of magnitude with respect to the situation without phase mismatch and by another factor of two to three when going from r = 3 to 10 μm. Figures S32–S33 of the SI describe the phase-matching effects on the polar maps of $\langle d_{eff} \rangle(\theta, \phi)$ for r = 3 μm and r = 10 μm.

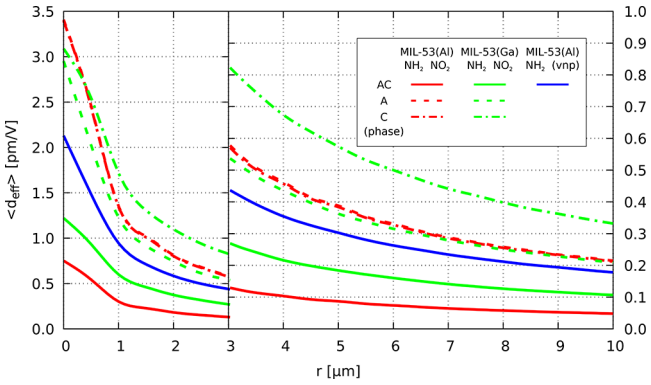

Figure 7. Grain size dependence of the calculated $\langle d_{eff} \rangle$ values for MIL-53(Al)-NH_2/NO_2, MIL-53(Ga)-NH_2/NO_2, and MIL-53(Al)-NH_2(vnp). For MIL-53(M)-NH_2/NO_2, results are listed for the pure A and C phases as well as for the A:C ratios obtained from PXRD analysis.

This ultimately leads to relatively low theoretical $\langle d_{eff} \rangle$ values for MIL-53(Al)-NH_2/NO_2 (**1**) and MIL-53(Ga)-NH_2/NO_2 (**3**), with respect to the potential $\chi^{(2)}$ or d_{eff} values if pure phase compounds could be created. Then, these final $\langle d_{eff} \rangle$ results, that is, when incorporating for all effects, show that the pure A and C phases of compound **1**/**2** and **3** are characterized by larger values of $\langle d_{eff} \rangle$ than compound **4** and that the differences between the A and C phases are larger for the Ga derivative. The comparison of these results with the experimental values also suggests that compound (**2**) is characterized by a much more ordered structure and thus higher $\chi^{(2)}$ than compound **1**.

The $\langle d_{eff} \rangle$ values for the optical path of 10 μm of the mixed AC phases of compound (**1**)/(**2**) (0.048 pm V^{-1}) and (**3**) (0.107 pm V^{-1}) and that of vnp structure of MIL-53(Al)-NH_2 (0.178 pm V^{-1}) compare quite well with experimental values (0.02, 0.02, and 0.05 pm V^{-1}, respectively). Although many effects were accounted for in the calculations, several factors need to be taken under consideration. First of all, the polydispersity of the studied materials hinders a direct comparison of the experimental value with single points (r values) of Figure 7.

The second important factor is the absorption of the SH signal and the associated resonance enhancement, larger in the case of MIL-53(Al/Ga)-NH_2/NO_2 species than in the case of the amino derivative. This could lead to a conclusion that the final results obtained for MIL-53(Al/Ga)-NH_2/NO_2 are somewhat underestimated and the true structure of these materials does not disfavor the $\chi^{(2)}$. Indeed, the overall values of the phase-matched mixed A/C crystals (0.75 pm V^{-1} for Al and 1.22 pm V^{-1} for Ga compound) are comparable to those of commercial inorganic NLO materials such as KDP (0.38–0.41 pm V^{-1} at 1064 nm), KTP (d_{eff} 1.7–3.5 pm V^{-1} at 800 nm) or BBO (d_{eff} 1.76–1.83 pm V^{-1} at 800 nm).[67] Moreover, the calculated $\chi^{(2)}$ tensors are considerable, which suggests that the investigated materials are of potential interest.

CONCLUSIONS

For the first time a polar organization of the well known PNA motif was achieved by incorporation of the motif in MOF structures. To be able to incorporate the motif in several MIL-53 MOFs, a linker was designed possessing an extended π-conjugated system with amino donor- and nitro acceptor-groups, as in PNA. Combining this linker with three different cations as nodes (Al, Ga, In), several MIL-53 frameworks were created. MIL-53(Al)-NH_2/NO_2 and MIL-53(Ga)-NH_2/NO_2 displayed a net polar and thus SHG-active organization of the linkers, whereas the MIL-53(In)-NH_2/NO_2 compound did not display SHG activity, indicating that no polar organization was obtained.

The SHG activity of the aluminum and gallium compounds was experimentally determined to be in the same range as that of the previously reported MIL-53(Al)-NH_2, where only an amino donor group resides on the terephthalate linker. Ab initio calculations revealed that while the terephthalate linker with the amino and nitro functionalization is more NLO efficient than the linker with sole amino functionalization, the occurrence of multiple phases of linker organization in MIL-53(M)-NH_2/NO_2 structures leads to partial cancellation of the SHG activity. Therefore, the SHG activities of MIL-53(Al)-NH_2/NO_2 and MIL-53(Ga)-NH_2/NO_2 lie in the same range as that of MIL-53(Al)-NH_2. Moreover, theoretical calculations revealed that the SHG activity of the MIL-53(M)-NH_2/NO_2 structures decreases with increasing grain size and that for the smallest grain size, where perfect phase matching occurs, the theoretical SHG activity is comparable to that of commercial inorganic NLO materials, such as KDP. This means that the investigated materials are of potential interest.

This research shows that the creation of MOFs containing linkers that mimic interesting SONLO properties of organic molecules in their motif can be a promising strategy to obtain functional polar crystals.

ASSOCIATED CONTENT

Supporting Information

The Supporting Information is available free of charge on the ACS Publications website at DOI: 10.1021/acs.jpcc.7b09190.

DOI: 10.1021/acs.jpcc.7b09190
J. Phys. Chem. C 2017, 121, 25509–25519

Detailed information about the linker synthesis, TG measurements, EA analyses, NMR spectra, and so on. (PDF)

AUTHOR INFORMATION

Corresponding Authors

*M.A.v.d.V.: Tel: + 31-15-2786458. E-mail: m.a.vanderveen@tudelft.nl.

*N.S.: Tel: + 49-431-8801675. E-mail: stock@ac.uni-kiel.de.

*B.C.: Tel: + 32-81-724554. E-mail: benoit.champagne@unamur.be.

ORCID

Helge Reinsch: 0000-0001-5288-1135

Benoît Champagne: 0000-0003-3678-8875

Norbert Stock: 0000-0002-0339-7352

Monique A. van der Veen: 0000-0002-0316-4639

Author Contributions

▽K.M., M.K., and T.S. contributed equally.

Funding

M.K. was financially supported by the Deutsche Forschungsgemeinschaft (DFG) (STO 643/10-1). K.M., T.S., D.E.D.V., and B.C. are grateful to Belspo for funding in the IAP project Functional Supramolecular Systems. D.E.D.V., T.V., and M.A.v.d.V. are grateful for the financial support from the Hercules Foundation and to FWO. This work was supported by funds from the Francqui Foundation (BC).The ab initio calculations were performed on the computers of the Consortium des Equipements de Calcul Intensif, including those of the Technological Platform of High-Performance Computing, for which we gratefully acknowledge the financial support of the FNRS-FRFC (convention nos. 2.4.617.07.F and 2.5020.11) and of the University of Namur. This research was supported in part by PL-Grid Infrastructure.

Notes

The authors declare no competing financial interest.

REFERENCES

(1) Ye, Z.-G. *Handbook of Dielectric, Piezoelectric and Ferroelectric Materials: Synthesis, Properties and Applications*; Woodhead Pub. and Maney Pub. on behalf of The Institute of Materials, Minerals & Mining, 2008.

(2) Curtin, D. Y.; Paul, I. C. Chemical Consequences of the Polar Axis in Organic Solid-State Chemistry. *Chem. Rev.* **1981**, *81*, 525−541.

(3) Asadi, K.; van der Veen, M. A. Ferroelectricity in Metal-Organic Frameworks: Characterization and Mechanisms. *Eur. J. Inorg. Chem.* **2016**, *2016*, 4332−4344.

(4) Fainman, Y.; Ma, J.; Lee, S. H. Non-Linear Optical Materials and Applications. *Mater. Sci. Rep.* **1993**, *9*, 53−139.

(5) Hollingsworth, M. D. Crystal Engineering: From Structure to Function. *Science* **2002**, *295*, 2410−2413.

(6) Mingabudinova, L. R.; Vinogradov, V. V.; Milichko, V. A.; Hey-Hawkins, E.; Vinogradov, A. V. Metal−Organic Frameworks as Competitive Materials for Non-Linear Optics. *Chem. Soc. Rev.* **2016**, *45*, 5408−5431.

(7) Evans, O. R.; Lin, W. Crystal Engineering of NLO Materials Based on Metal−Organic Coordination Networks. *Acc. Chem. Res.* **2002**, *35*, 511−522.

(8) Shi, Y.; Zhang, C.; Zhang, H.; Bechtel, J. H.; Dalton, L. R.; Robinson, B. H.; Steier, W. H. Low (Sub-1-V) Halfwave Voltage Polymeric Electro-Optic Modulators Achieved by Controlling Chromophore Shape. *Science* **2000**, *288*, 119−122.

(9) Burland, D. M.; Miller, R. D.; Walsh, C. A. Second-Order Nonlinearity in Poled-Polymer Systems. *Chem. Rev.* **1994**, *94*, 31−75.

(10) Marks, T. J.; Ratner, M. A. Design, Synthesis, and Properties of Molecule-Based Assemblies with Large Second-Order Optical Nonlinearities. *Angew. Chem., Int. Ed. Engl.* **1995**, *34*, 155−173.

(11) Ashwell, G. J.; Jackson, P. D.; Crossland, W. A. Non-Centrosymmetry and Second-Harmonic Generation in Z-Type Langmuir-Blodgett Films. *Nature* **1994**, *368*, 438−440.

(12) Penner, T. L.; Motschmann, H. R.; Armstrong, N. J.; Ezenyilimba, M. C.; Williams, D. J. Efficient Phase-Matched Second-Harmonic Generation of Blue Light in an Organic Waveguide. *Nature* **1994**, *367*, 49−51.

(13) Lin, W. W.; Lin, W. W.; Wong, G. K.; Marks, T. J. Supramolecular Approaches to Second-Order Nonlinear Optical Materials. Self-Assembly and Microstructural Characterization of Intrinsically Acentric [(Aminophenyl)azo]pyridinium Superlattices. *J. Am. Chem. Soc.* **1996**, *118*, 8034−8042.

(14) Katz, H. E.; Wilson, W. L.; Scheller, G. Chromophore Structure, Second Harmonic Generation, and Orientational Order in Zirconium Phosphonate/Phosphate Self-Assembled Multilayers. *J. Am. Chem. Soc.* **1994**, *116*, 6636−6640.

(15) Zyss, J.; Nicoud, J. F.; Coquillay, M. Chirality and Hydrogen Bonding in Molecular Crystals for Phase-Matched Second-Harmonic Generation: N-(4-Nitrophenyl)-(L)-Prolinol (NPP). *J. Chem. Phys.* **1984**, *81*, 4160.

(16) Gryl, M.; Krawczuk, A.; Stadnicka, K. Polymorphism of Urea-Barbituric Acid Co-Crystals. *Acta Crystallogr., Sect. B: Struct. Sci.* **2008**, *64*, 623−632.

(17) Gryl, M.; Kozieł, M.; Stadnicka, K.; Matulková, I.; Němec, I.; Tesařová, N.; Němec, P. Lidocaine Barbiturate: A Promising Material for Second Harmonic Generation. *CrystEngComm* **2013**, *15*, 3275.

(18) Gryl, M.; Seidler, T.; Stadnicka, K.; Matulkova, I.; Nemec, I.; Tesarova, N.; Nemec, P. The Crystal Structure and Optical Properties of a Pharmaceutical Co-Crystal - the Case of the Melamine-Barbital Addition Compound. *CrystEngComm* **2014**, *16*, 5765−5768.

(19) Evans, O. R.; Xiong, R.; Wang, Z.; Wong, G. K.; Lin, W. Crystal Engineering of Acentric Diamondoid Metal-Organic Coordination Networks. *Angew. Chem., Int. Ed.* **1999**, *38*, 536−538.

(20) Mendiratta, S.; Lee, C. H.; Lee, S. Y.; Kao, Y. C.; Chang, B. C.; Lo, Y. H.; Lu, K. L. Structural Characteristics and Non-Linear Optical Behaviour of a 2-Hydroxynicotinate-Containing Zinc-Based Metal-Organic Framework. *Molecules* **2015**, *20*, 8941−8951.

(21) Serra-Crespo, P.; van der Veen, M. A.; Gobechiya, E.; Houthoofd, K.; Filinchuk, Y.; Kirschhock, C. E. A.; Martens, J. A.; Sels, B. F.; De Vos, D. E.; Kapteijn, F.; et al. NH_2-MIL-53(Al): A High-Contrast Reversible Solid-State Nonlinear Optical Switch. *J. Am. Chem. Soc.* **2012**, *134*, 8314−8317.

(22) Jain, P.; Dalal, N. S.; Toby, B. H.; Kroto, H. W.; Cheetham, A. K. Order-Disorder Antiferroelectric Phase Transition in a Hybrid Inorganic-Organic Framework with the Perovskite Architecture. *J. Am. Chem. Soc.* **2008**, *130*, 10450−10451.

(23) Jain, P.; Ramachandran, V.; Clark, R. J.; Zhou, H. D.; Toby, B. H.; Dalal, N. S.; Kroto, H. W.; Cheetham, A. K. Multiferroic Behavior Associated with an Order−Disorder Hydrogen Bonding Transition in Metal−Organic Frameworks (MOFs) with the Perovskite ABX_3 Architecture. *J. Am. Chem. Soc.* **2009**, *131*, 13625−13627.

(24) Zhang, W.; Cai, Y.; Xiong, R. G.; Yoshikawa, H.; Awaga, K. Exceptional Dielectric Phase Transitions in a Perovskite-Type Cage Compound. *Angew. Chem., Int. Ed.* **2010**, *49*, 6608−6610.

(25) Xu, G.-C.; Ma, X.-M.; Zhang, L.; Wang, Z.-M.; Gao, S. Disorder-Order Ferroelectric Transition in the Metal Formate Framework of $[NH_4][Zn(HCOO)_3]$. *J. Am. Chem. Soc.* **2010**, *132*, 9588−9590.

(26) Cui, H.; Zhou, B.; Long, L.-S.; Okano, Y.; Kobayashi, H.; Kobayashi, A. A Porous Coordination-Polymer Crystal Containing One-Dimensional Water Chains Exhibits Guest-Induced Lattice Distortion and a Dielectric Anomaly. *Angew. Chem., Int. Ed.* **2008**, *47*, 3376−3380.

(27) Dong, X.-Y.; Li, B.; Ma, B.-B.; Li, S.-J.; Dong, M.-M.; Zhu, Y.-Y.; Zang, S.-Q.; Song, Y.; Hou, H.-W.; Mak, T. C. W. Ferroelectric Switchable Behavior through Fast Reversible De/adsorption of Water

DOI: 10.1021/acs.jpcc.7b09190
J. Phys. Chem. C 2017, 121, 25509−25519

Spirals in a Chiral 3D Metal-Organic Framework. *J. Am. Chem. Soc.* **2013**, *135*, 10214−10217.
(28) Markey, K.; Putzeys, T.; Horcajada, P.; Devic, T.; Guillou, N.; Wübbenhorst, M.; Van Cleuvenbergen, S.; Verbiest, T.; De Vos, D. E.; van der Veen, M. A.; et al. Second Harmonic Generation Microscopy Reveals Hidden Polar Organization in Fluoride Doped MIL-53(Fe). *Dalt. Trans.* **2016**, *45*, 4401−4406.
(29) Abrahams, S. C.; Robertson, J. M. The Crystal Structure of *P*-Nitroaniline, $NO_2.C_6H_4.NH_2$. *Acta Crystallogr.* **1948**, *1*, 252−259.
(30) Donohue, J.; Trueblood, K. The Crystal Structure of *P*-Nitroaniline. *Acta Crystallogr.* **1956**, *9*, 960−965.
(31) Wübbenhorst, M.; Klap, G. J.; Jansen, J. C.; van Bekkum, H.; van Turnhout, J. Glass Transition of One-Dimensional Molecular Chains of *P*-Nitroaniline Confined in AlPO4−5 Nanopores Revealed by Dielectric Spectroscopy. *J. Chem. Phys.* **1999**, *111*, 5637−5640.
(32) van der Veen, M. A.; Van Noyen, J.; Sels, B. F.; Jacobs, P. A.; Verbiest, T.; De Vos, D. E. Mapping of the Organization of *P*-Nitroaniline in SAPO-5 by Second-Harmonic Generation Microscopy. *Phys. Chem. Chem. Phys.* **2010**, *12*, 10688.
(33) van der Veen, M. A.; Sels, B. F.; De Vos, D. E.; Verbiest, T. Localization of *P*-Nitroaniline Chains Inside Zeolite ZSM-5 with Second-Harmonic Generation Microscopy. *J. Am. Chem. Soc.* **2010**, *132*, 6630−6631.
(34) Marlow, F.; Wübbenhorst, M.; Caro, J. Pyroelectric Effects on Molecular Sieve Crystals Loaded with Dipole Molecules. *J. Phys. Chem.* **1994**, *98*, 12315−12319.
(35) Klap, G. J.; van Klooster, S. M.; Wübbenhorst, M.; Jansen, J. C.; van Bekkum, H.; van Turnhout, J. Polarization Reversal in $AlPO_4$-5 Crystals Containing Polar or Nonpolar Organic Molecules: A Scanning Pyroelectric Microscopy Study. *J. Phys. Chem. B* **1998**, *102*, 9518−9524.
(36) Klap, G. J.; Wübbenhorst, M.; Jansen, J. C.; van Koningsveld, H.; van Bekkum, H.; van Turnhout, J. Polar Growth and Directional Adsorption of Large $AlPO_4$-5 Crystals Determined by Scanning Pyroelectric Microscopy. *Chem. Mater.* **1999**, *11*, 3497−3503.
(37) Skibo, E. B.; Gilchrist, J. H. Synthesis and Electrochemistry of Pyrimidoquinazoline-5,10-Diones. Design of Hydrolytically Stable High Potential Quinones and New Reductive Alkylation Systems. *J. Org. Chem.* **1988**, *53*, 4209−4218.
(38) Stock, N. Hochdurchsatzmethoden Zur Entdeckung Und Optimierung Kristalliner Poröser Materialien. *Chem. Ing. Tech.* **2010**, *82*, 1039−1047.
(39) Stock, N. High-Throughput Investigations Employing Solvothermal Syntheses. *Microporous Mesoporous Mater.* **2010**, *129*, 287−295.
(40) Stock, N.; Biswas, S. Synthesis of Metal-Organic Frameworks (MOFs): Routes to Various MOF Topologies, Morphologies, and Composites. *Chem. Rev.* **2012**, *112*, 933−969.
(41) Bauer, S.; Stock, N. Hochdurchsatz-Methoden in Der Festkörperchemie. Schneller Zum Ziel. Chem. *Chem. Unserer Zeit* **2007**, *41*, 390−398.
(42) *Topas Academic 4.2*; Coelho Software: Brisbane, Australia, 2007.
(43) Loiseau, T.; Serre, C.; Huguenard, C.; Fink, G.; Taulelle, F.; Henry, M.; Bataille, T.; Férey, G. A Rationale for the Large Breathing of the Porous Aluminum Terephthalate (MIL-53) Upon Hydration. *Chem. - Eur. J.* **2004**, *10*, 1373−1382.
(44) *Materials Studio*, version 5.0; Accelrys Software, Inc., 2009.
(45) Dovesi, R.; Orlando, R.; Erba, A.; Zicovich-Wilson, C. M.; Civalleri, B.; Casassa, S.; Maschio, L.; Ferrabone, M.; De La Pierre, M.; D'Arco, P.; et al. CRYSTAL14: A Program for the Ab Initio Investigation of Crystalline Solids. *Int. J. Quantum Chem.* **2014**, *114*, 1287−1317.
(46) Dovesi, R.; Saunders, V. R.; Roetti, C.; Orlando, R.; Zicovich-Wilson, C. M.; Pascale, F.; Civalleri, B.; Doll, K.; Harrison, N. M.; Bush, I. J.; et al.. *CRYSTAL14 User's Manual*; University of Torino: Torino, Italy, 2014.
(47) Seidler, T.; Champagne, B. Which Charge Definition for Describing the Crystal Polarizing Field and the $\chi^{(1)}$ and $\chi^{(2)}$ of Organic Crystals? *Phys. Chem. Chem. Phys.* **2015**, *17*, 19546−19556.
(48) Seidler, T.; Champagne, B. Second-Order Nonlinear Optical Susceptibilities of Metal−Organic Frameworks Using a Combined Local Field Theory/Charge Embedding Electrostatic Scheme. *J. Phys. Chem. C* **2016**, *120*, 6741−6749.
(49) Frisch, M. J.; Trucks, G. W.; Schlegel, H. B.; Scuseria, G. E.; Robb, M. A.; Cheeseman, J. R.; Scalmani, G.; Barone, V.; Mennucci, B.; Petersson, G. A.; et al. *Gaussian 09*, revision B.01; Gaussian, Inc.: Wallingford, CT, 2009.
(50) MUNN, R. W. A. General Microscopic Theory of Bulk Second-Harmonic Generation from Molecular Crystals. *Mol. Phys.* **1996**, *89*, 555−569.
(51) Kirtman, B.; Dykstra, C. E.; Champagne, B. Major Intermolecular Effects on Nonlinear Electrical Response in a Hexatriene Model of Solid State Polyacetylene. *Chem. Phys. Lett.* **1999**, *305*, 132−138.
(52) Reis, H.; Papadopoulos, M. G.; Calaminici, P.; Jug, K.; Köster, A. M. Calculation of Macroscopic Linear and Nonlinear Optical Susceptibilities for the Naphthalene, Anthracene and Meta-Nitroaniline Crystals. *Chem. Phys.* **2000**, *261*, 359−371.
(53) Seidler, T.; Stadnicka, K.; Champagne, B. Investigation of the Linear and Second-Order Nonlinear Optical Properties of Molecular Crystals within the Local Field Theory. *J. Chem. Phys.* **2013**, *139*, 114105.
(54) Seidler, T.; Stadnicka, K.; Champagne, B. Second-Order Nonlinear Optical Susceptibilities and Refractive Indices of Organic Crystals from a Multiscale Numerical Simulation Approach. *Adv. Opt. Mater.* **2014**, *2*, 1000−1006.
(55) Seidler, T.; Stadnicka, K.; Champagne, B. Evaluation of the Linear and Second-Order NLO Properties of Molecular Crystals within the Local Field Theory: Electron Correlation Effects, Choice of XC Functional, ZPVA Contributions, and Impact of the Geometry in the Case of 2-Methyl-4-Nitroaniline. *J. Chem. Theory Comput.* **2014**, *10*, 2114−2124.
(56) Seidler, T.; Stadnicka, K.; Champagne, B. Linear and Second-Order Nonlinear Optical Properties of Ionic Organic Crystals. *J. Chem. Phys.* **2014**, *141*, 104109.
(57) Wittmann, T.; Siegel, R.; Reimer, N.; Milius, W.; Stock, N.; Senker, J. Enhancing the Water Stability of Al-MIL-101-NH_2 via Postsynthetic Modification. *Chem. - Eur. J.* **2015**, *21*, 314−323.
(58) Ahnfeldt, T.; Gunzelmann, D.; Loiseau, T.; Hirsemann, D.; Senker, J.; Férey, G.; Stock, N. Synthesis and Modification of a Functionalized 3D Open-Framework Structure with MIL-53 Topology. *Inorg. Chem.* **2009**, *48*, 3057−3064.
(59) Sumida, K.; Rogow, D. L.; Mason, J. A.; McDonald, T. M.; Bloch, E. D.; Herm, Z. R.; Bae, T.; Long, J. R. Carbon Dioxide Capture in Metal−Organic Frameworks. *Chem. Rev.* **2012**, *112*, 724−781.
(60) Serra-Crespo, P.; Gobechiya, E.; Ramos-Fernandez, E. V.; Juan-Alcañiz, J.; Martinez-Joaristi, A.; Stavitski, E.; Kirschhock, C. E. a.; Martens, J. a.; Kapteijn, F.; Gascon, J. Interplay of Metal Node and Amine Functionality in NH_2-MIL-53: Modulating Breathing Behavior through Intra-Framework Interactions. *Langmuir* **2012**, *28*, 12916−12922.
(61) Boyd, R. W. *Nonlinear Optics*; Elsevier, 2008.
(62) Le Floc'h, V.; Brasselet, S.; Roch, J.-F.; Zyss, J. Monitoring of Orientation in Molecular Ensembles by Polarization Sensitive Nonlinear Microscopy. *J. Phys. Chem. B* **2003**, *107*, 12403−12410.
(63) Loiseau, T.; Muguerra, H.; Haouas, M.; Taulelle, F.; Férey, G. Hydrothermal Synthesis and Structural Characterization of a Gallium Pyromellitate Ga(OH)(btec)·0.5H_2O, with Infinite Ga-(μ_2-OH)-Ga Chains (MIL-61). *Solid State Sci.* **2005**, *7*, 603−609.
(64) Gándara, F.; Gomez-Lor, B.; Gutiérrez-Puebla, E.; Iglesias, M.; Monge, M. A.; Proserpio, D. M.; Snejko, N. An Indium Layered MOF as Recyclable Lewis Acid Catalyst. *Chem. Mater.* **2008**, *20*, 72−76.
(65) Van Der Veen, M. A.; Verbiest, T.; De Vos, D. E. Probing Microporous Materials with Second-Harmonic Generation. *Microporous Mesoporous Mater.* **2013**, *166*, 102−108.
(66) Falaise, C.; Volkringer, C.; Facqueur, J.; Bousquet, T.; Gasnot, L.; Loiseau, T. Capture of Iodine in Highly Stable Metal−Organic Frameworks: A Systematic Study. *Chem. Commun.* **2013**, *49*, 10320.

DOI: 10.1021/acs.jpcc.7b09190
J. Phys. Chem. C 2017, 121, 25509−25519

(67) Armstrong, D. J.; Alford, W. J.; Raymond, T. D.; Smith, A. V. Absolute Measurement of the Effective Nonlinearities of KTP and BBO Crystals by Optical Parametric Amplification. *Appl. Opt.* **1996**, *35*, 2032−2040.

DOI: 10.1021/acs.jpcc.7b09190
J. Phys. Chem. C 2017, 121, 25509−25519